

Origin of low thermal conductivity in SnSe

Yu Xiao,¹ Cheng Chang,¹ Yanling Pei,¹ Di Wu,^{2,3} Kunling Peng,⁴ Xiaoyuan Zhou,⁴ Shengkai Gong,¹ Jiaqing He,^{2,3}
 Yongsheng Zhang,^{5,6,*} Zhi Zeng,^{5,6} and Li-Dong Zhao^{1,†}

¹School of Materials Science and Engineering, Beihang University, Beijing 100191, China

²Department of Physics, South University of Science and Technology of China, Shenzhen 518055, China

³Shenzhen Key Laboratory of Thermoelectric Materials, Shenzhen 518055, China

⁴College of Physics, Chongqing University, Chongqing 401331, China

⁵Key Laboratory of Materials Physics, Institute of Solid State Physics, Chinese Academy of Sciences, Hefei 230031, China

⁶University of Science and Technology of China, Hefei 230026, China

(Received 2 April 2016; revised manuscript received 22 July 2016; published 12 September 2016)

We provide direct evidence to understand the origin of low thermal conductivity of SnSe using elastic measurements. Compared to state-of-the-art lead chalcogenides PbQ ($Q = Te, Se, S$), SnSe exhibits low values of sound velocity (~ 1420 m/s), Young's modulus ($E \sim 27.7$ GPa), and shear modulus ($G \sim 9.6$ GPa), which are ascribed to the extremely weak Sn-Se atomic interactions (or bonds between layers); meanwhile, the deduced average Grüneisen parameter γ of SnSe is as large as ~ 3.13 , originating from the strong anharmonicity of the bonding arrangement. The calculated phonon mean free path ($l \sim 0.84$ nm) at 300 K is comparable to the lattice parameters of SnSe, indicating little room is left for further reduction of the thermal conductivity through introducing nanoscale microstructures and microscale grain boundaries. The low elastic properties indicate that the weak chemical bonding stiffness of SnSe generally causes phonon modes softening which eventually slows down phonon propagation. This work provides insightful data to understand the low lattice thermal conductivity of SnSe.

DOI: 10.1103/PhysRevB.94.125203

Thermoelectric materials, which could harvest waste heat and convert into electricity, are regarded as an alternative choice for future power generation. The efficiency of a thermoelectric material is determined by the dimensionless figure of merit (ZT), defined as $ZT = (S^2\sigma T)/\kappa$, where S is the Seebeck coefficient, σ is electrical conductivity, κ is thermal conductivity, and T is working temperature. Ideally, both Seebeck coefficient S and electrical conductivity σ must be large while thermal conductivity κ must be minimized [1,2]. To date, approaches to enhance ZT are mainly divided into power factor enhancement [3–5] and thermal conductivity reduction [6,7]. In practice, it is challenging to develop an effective approach to improve the individual parameters simultaneously owing to their complex interrelationship [8,9], although the lattice thermal conductivity (κ_{lat}), determined by the lattice bonding, is believed to be the only near-independent parameter for ZT tuning [10]. In the last decade, nanostructuring (matrix or second phase nanoprecipitates) and all-scale hierarchical architecturing have been developed to be the most effective approaches to reduce lattice thermal conductivity. In addition, a single-phase compound with low thermal conductivity would be a decent alternative [11–14]. The most appealing advantage of this type of compound is that these complex procedures (nanostructuring and hierarchical architecturing, for example) to reduce the thermal conductivity can be avoided. Typically, a low thermal conductivity may arise from strong crystal anharmonicity [12,15–18], complex crystal structure [19], atomic disorders induced by mobile ions such as copper and silver ions and their liquidlike behaviors

[20,21], large molecular weight [22], large unit cells [23], or lone-pair electrons [24], etc.

Recently, the achievements in SnSe crystals have triggered intense research enthusiasm in the thermoelectric community. High thermoelectric performance was exhibited in hole-doped single-crystalline SnSe over a broad temperature range originating from both an ultrahigh power factor and ultralow thermal conductivity [12,25–29]. The low thermal conductivity of SnSe was explained by strong anharmonicity in terms of large Grüneisen parameters via density functional theory (DFT) calculations [12], while this strong anharmonicity is attributed to the weak Sn-Se atomic interactions (or bonds), which has recently been experimentally confirmed by inelastic neutron scattering (INS) measurements [17]. Heremans [16] used a simple ball-and-spring model to describe the relationship between the bond strength and anharmonicity, implying that the weak atomic bonds usually lead to strong anharmonicity. Despite these reasonable qualitative physical pictures and analysis [17], no quantitative account of the ultralow thermal conductivity in SnSe crystals has been given so far. In this work, to explore the origin of low thermal conductivity of SnSe, we carried out the elastic property evaluations through ultrasonic pulse echo measurements and first-principles calculations. PbQ ($Q = Te, Se, S$) compounds have been widely studied in the thermoelectric community and $PbTe$ shows low thermal conductivity due to the shift of Pb [30,31]. Compared to state-of-art PbQ ($Q = Te, Se, S$), SnSe exhibits much lower elastic properties including average sound velocity (v_a), Young's modulus (E) and shear modulus (G); meanwhile, possesses larger Grüneisen parameter (γ), and lower Debye temperature (θ_D) and shorter phonon mean free path (ℓ). Low elastic properties indicate a weak chemical bonding stiffness of SnSe, which generally causes phonon mode softening and slows down phonon propagation.

*Corresponding author: yshzhang@theory.issp.ac.cn

†Corresponding author: zhaolidong@buaa.edu.cn

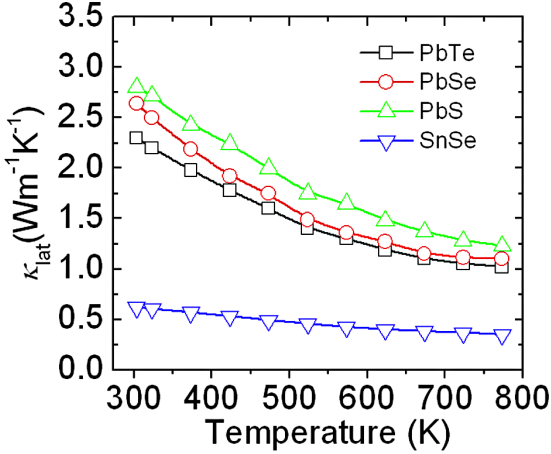


FIG. 1. The lattice thermal conductivity κ_{lat} of SnSe and $\text{Pb}Q$ ($Q = \text{Te}, \text{Se}, \text{and S}$).

SnSe and $\text{Pb}Q$ ($Q = \text{Te}, \text{Se}, \text{and S}$) crystals were prepared using the Bridgman method. See the Supplemental Material for experimental details [32,33]. The longitudinal and shear acoustic velocities were measured using an ultrasonic instrument (Ultrasonic Pulser/Receiver Model 5058 PR, Olympus, USA). Figure S1 in the Supplemental Material [32] shows the schematic diagram of ultrasonic pulse echo measurements. The shear wave velocity v_s and longitudinal wave velocity v_l can be derived from the thickness of sample D and travel time Δt . In this work, the sample was polished to a thickness of 1–2 mm. For the density functional theory (DFT) calculations, we used the Vienna *Ab Initio* Simulation Package (VASP) [34] with the projector augmented wave (PAW) scheme, and the generalized gradient approximation of Perdew, Burke, and Ernzerhof (GGA-PBE) [35] for the electronic exchange-correlation functional. See the Supplemental Material [32] for theoretical calculations [34–38].

The temperature dependence of lattice thermal conductivities (κ_{lat}) for SnSe and $\text{Pb}Q$ ($Q = \text{Te}, \text{Se}, \text{S}$) are shown in Fig. 1. At room temperature, the lattice thermal conductivities are $\sim 0.62 \text{ W m}^{-1} \text{ K}^{-1}$ for SnSe along the b axis (the discussion in this work is hereafter restricted to the b axis since it showed the highest performance), and keeps a decreasing trend with rising temperature and eventually falls to $\sim 0.3 \text{ W m}^{-1} \text{ K}^{-1}$ at 773 K. In comparison, the room temperature lattice thermal conductivities are 2.3, 2.64, and $2.8 \text{ W m}^{-1} \text{ K}^{-1}$ for PbTe, PbSe, and PbS, respectively. The low thermal conductivity in SnSe was ascribed to the high crystal anharmonicity attributed to the weak atomic bonds, which were supported by the density functional theory (DFT) calculations [11] and related to the electronic orbitals (Se 4p bonds coupled to two 5s electrons of Sn as lone-pair electrons) of SnSe [16,17].

Elastic properties are widely used to evaluate the interatomic bonding strength and lattice vibration anharmonicity in a crystal lattice. Usually, low Young's modulus, shear modulus, and large Grüneisen parameter imply a low lattice thermal conductivity [23,39–41]. The thermal conductivity (κ) is related to Young's modulus (E), Grüneisen parameter (γ), and Debye temperature (θ_D) via the formula as follows

[42,43]:

$$\kappa = \frac{3.0 \times 10^{-5} \overline{M}_a a \theta_D^3}{T \gamma^2 v^{2/3}}, \quad (1)$$

$$\kappa \propto \frac{\rho^{1/6} E^{1/2}}{(M/m)^{3/2}}, \quad (2)$$

where ρ is the sample density, \overline{M}_a is the mean atomic weight of all the constituent atoms, a^3 is the average volume occupied by one atom, v is the number of atoms in the unit primitive cell, M is the atomic weight of the molecule of the compound, and m is the number of atoms in the molecule. As shown above, Eqs. (1) and (2) summarize the key-variable interconnections quite nicely.

In this work, average sound velocity (v_a), Young's modulus (E), shear modulus (G), Poisson ratio v_p , and Grüneisen parameter (γ) can be calculated from the sound velocity as follows [23,43–47]:

$$v_a = \left[\frac{1}{3} \left(\frac{1}{v_l^3} + \frac{2}{v_s^3} \right) \right]^{-1/3}, \quad (3)$$

$$E = \frac{\rho v_s^2 (3v_l^2 - 4v_s^2)}{(v_l^2 - v_s^2)}, \quad (4)$$

$$v_p = \frac{1 - 2(v_s/v_l)}{2 - 2(v_s/v_l)^2}, \quad (5)$$

$$G = \frac{E}{2(1 + v_p)}, \quad (6)$$

$$\gamma = \frac{3}{2} \left(\frac{1 + v_p}{2 - 3v_p} \right), \quad (7)$$

where v_l and v_s denote longitudinal and shear sound velocities, respectively. The sound velocity can be acquired directly in the ultrasonic pulse echo measurements, shown in Table I. The sound velocity in SnSe was measured along the b axis; however, the sound velocity in the $\text{Pb}Q$ ($Q = \text{Te}, \text{Se}, \text{S}$) system having an isotropic crystal structure is measured in an arbitrary axis. As seen in Table I, the calculated Poisson ratio of SnSe using the experimentally measured velocities is larger than those $\text{Pb}Q$ ($Q = \text{Te}, \text{Se}, \text{S}$), which indicates that SnSe could experience large deformation under stress. What is more, the average sound velocity (v_a), Young's modulus (E), and shear modulus (G) of SnSe are much lower than those of $\text{Pb}Q$ ($Q = \text{Te}, \text{Se}, \text{S}$). The low Young's modulus (27.7 GPa) and shear modulus (9.6 GPa) of SnSe are consistent with the low average sound velocity $v_a \sim 1420 \text{ m s}^{-1}$. To make comparisons with experimental data, we also conducted first-principles density functional theory (DFT) phonon calculations on the phonon dispersions of SnSe and $\text{Pb}Q$ ($Q = \text{Te}, \text{Se}, \text{S}$) (Fig. 2). As seen, the highest acoustic mode boundary frequencies of SnSe, PbTe, PbSe, and PbS are 50, 87, 98, and 103 cm^{-1} , respectively, suggesting the mode softening is most severe in SnSe. The longitudinal and shear sound velocities are derived from the slope of three acoustic phonon dispersions around the Γ point, and are in good agreement with the experimental measurements. Moreover, the elastic properties of the four

TABLE I. The experimentally measured lattice thermal conductivity (κ_L) and sound velocity (v_l, v_s, v_a) of SnSe and Pb Q ($Q = \text{Te}, \text{Se}$, and S) at 300 K. The elastic properties (E , G , and v_p) and the Grüneisen parameter (γ) are derived based on Eqs. (4)–(7) using the sound velocities. Data within parentheses are DFT calculated elastic properties (E , G , and v_p), thermal properties (v_l, v_s, v_a , and θ_D drawn from the phonon dispersions, Fig. 2), and anharmonic property (γ calculated using the quasiharmonic approximation, Fig. 3).

Parameters	SnSe	PbTe	PbSe	PbS
Lattice thermal conductivity, $\kappa_L(\text{W m}^{-1}\text{K}^{-1})$	0.62	2.30	2.64	2.80
Longitudinal sound velocity, $v_l(\text{m s}^{-1})$	2730 (2878)	2910 (2598)	3200 (3021)	3450 (3290)
Shear sound velocity, $v_s(\text{m s}^{-1})$	1250 (1465)	1610 (1636)	1750 (1749)	1900 (1995)
Average sound velocity, $v_a(\text{m s}^{-1})$	1420 (1641)	1794 (1800)	1951 (1941)	2118 (2205)
Young's modulus, E (GPa)	27.7 (40.5)	54.1 (53.7)	65.2 (62.2)	70.2 (69.7)
Shear modulus, G (GPa)	9.6 (14.5)	21.1 (21.2)	25.3 (24.3)	27.4 (27.2)
Poisson ratio, v_p	0.44 (0.37)	0.28 (0.26)	0.29 (0.28)	0.28 (0.28)
Grüneisen parameter, γ	3.13 (2.83)	1.65 (1.49)	1.69 (2.66)	1.67 (2.46)
Phonon mean free path, l (nm)	0.84	3.10	2.72	2.44
Debye temperature, θ_D (K)	142 (132)	164 (172)	190 (220)	213 (253)

compounds were calculated using DFT and the theoretical elastic properties (Young's modulus, shear modulus, and Poisson ratio) are also consistent with the experimental measurements.

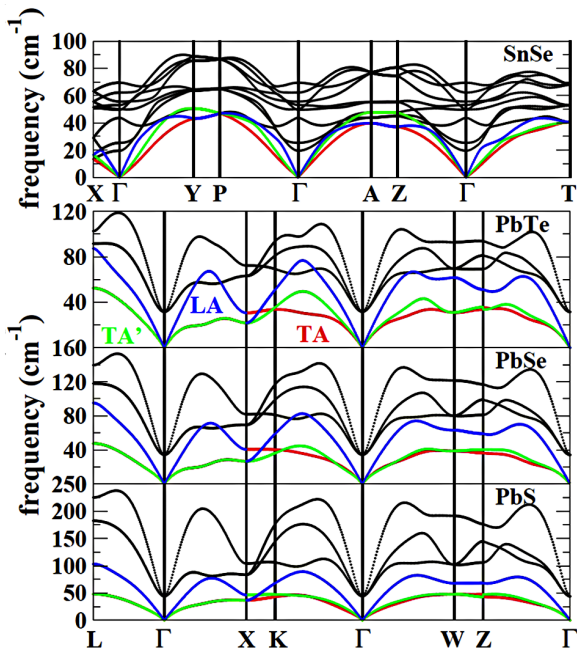


FIG. 2. The theoretically calculated phonon dispersions of SnSe, PbTe, PbSe, and PbS. The red, green, and blue lines highlight two transverse (TA, TA'), and one longitudinal (LA) acoustic modes, respectively.

Usually, a large Grüneisen parameter reflects a strong crystal anharmonicity, hence a low thermal conductivity. The Grüneisen parameter $\gamma \sim 3.13$ of SnSe, derived from the longitudinal and shear sound velocities, is much higher than those of lead chalcogenides, namely, ~ 1.65 , ~ 1.69 , and ~ 1.67 for PbTe, PbSe, and PbS, respectively (Table I). The results are confirmed by the density functional calculated for the Grüneisen parameters of the four compounds (SnSe, PbTe, PbSe, and PbS) within quasiharmonic approximation (Fig. 3). In contrast, Grüneisen parameters are ~ 2.05 for AgSbTe₂ and ~ 3.5 for AgSbSe₂ at room temperature, corresponding to measured lattice thermal conductivity at room temperature of $0.68 \text{ W m}^{-1}\text{K}^{-1}$ and $0.48 \text{ W m}^{-1}\text{K}^{-1}$, respectively. It was argued that the strong anharmonicity of AgSbTe₂ and AgSbSe₂ comes from the lone-pair electrons at Sb sites [13,48]. In SnSe, the strong anharmonicity is ascribed to the electrostatic repulsion between Sn 5s lone-pair electrons and its special crystal structures (see below).

Apart from these elastic parameters (sound velocity, Young's modulus, shear modulus, and Grüneisen parameters), the value of Debye temperature also reflects the thermal conductivity to some extent. Debye temperature θ_D can be estimated as follows [13,23]:

$$\theta_D = \frac{h}{k_B} \left[\frac{3N}{4\pi V} \right]^{1/3} v_a, \quad (8)$$

where h is Planck's constant, k_B is the Boltzmann constant, N is the number of atoms in a unit cell, V is the unit-cell volume, and v_a is the average sound velocity. As shown in Fig. 4 (a), the Debye temperature $\theta_D \sim 142 \text{ K}$ of SnSe is smaller than $\sim 164 \text{ K}$ for PbTe, $\sim 190 \text{ K}$ for PbSe, and $\sim 213 \text{ K}$ for

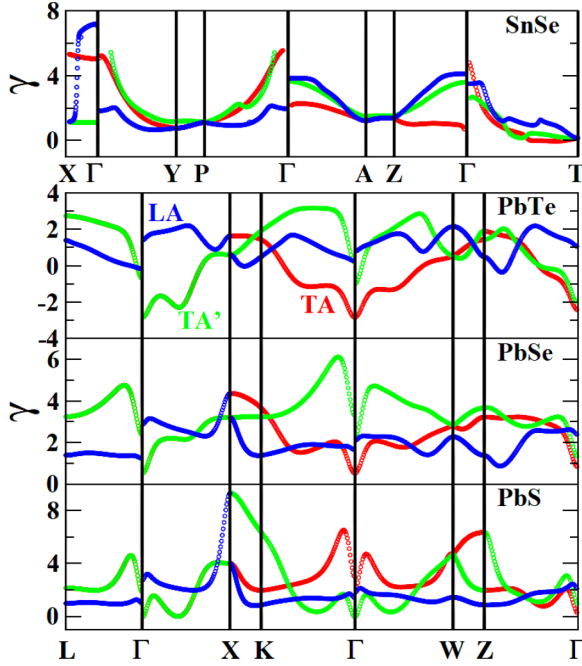


FIG. 3. The quasiharmonic phonon calculated Grüneisen dispersions of SnSe, PbTe, PbSe, and PbS. The red, green, and blue lines highlight two transverse (TA, TA'), and one longitudinal (LA) acoustic modes, respectively.

PbS. The Debye temperatures of the four compounds evaluated using the average sound velocity [Eq. (8)] are in reasonable agreement with the theoretical values (Table I) estimated using the phonon dispersions (Fig. 2). Obviously, the low Debye temperature is a clear reflection of the low lattice thermal conductivity in the SnSe system. To further prove the low Debye temperature, we carried out a low-temperature specific heat C_p measurement, as shown in Fig. 4(b). According to the temperature dependence of the specific heat curve, C_p comes close to a constant after reaching ~ 135 K, which is in good accordance with the low Debye temperature ~ 142 K derived from the elastic measurements. The low Debye temperature of SnSe is comparable to 125 and 135 K for AgSbTe₂ and AgBiSe₂ respectively [13].

Usually, the materials with low thermal conductivity possess very short phonon mean free path (MFP). We evaluate the phonon mean free path l using the following equation [13,48]:

$$\kappa_{\text{lat}} = \frac{1}{3} C_v v_a l, \quad (9)$$

where C_v represents the heat capacity at constant volume, which can be substituted by $C_v = C_p \rho / (C_p)$ (C_p is heat capacity at constant pressure and ρ is sample density). The phonon mean free path of SnSe, $l \sim 0.84$ nm, is much shorter than those of lead chalcogenides Pb Q ($Q = \text{Te, Se, S}$), as shown in Table I. The MFP of SnSe is comparable to the lattice parameters of the unit cell in the *Pnma* phase ($a = 11.49$ Å, $b = 4.135$ Å, $c = 4.44$ Å), implying that the phonon propagation in SnSe is mainly determined by the umklapp processes and point defects, and that using nanoscale microstructures and microscale grain boundaries to reduce lattice thermal conductivity in SnSe is probably in vain.

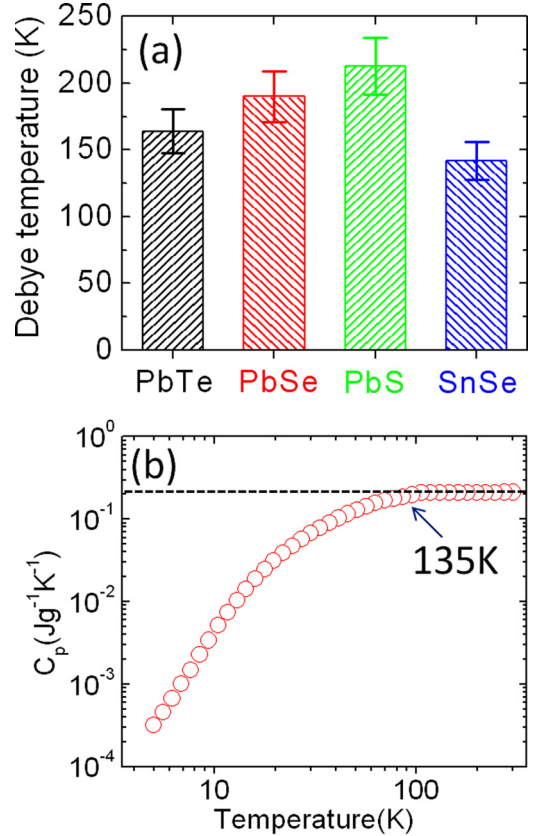


FIG. 4. (a) Debye temperature θ_D of Pb Q ($Q = \text{Te, Se, S}$) and SnSe; (b) the temperature dependence of specific heat capacity C_p of SnSe. Based on the Debye model, the specific heat capacity C_p will reach a constant when temperature increases up to the θ_D , therefore, the θ_D of SnSe can be directly acquired using low-temperature specific heat measurements [13].

The present results indicate that the crystal structure related elastic behaviors including Young's modulus, shear modulus, and Grüneisen parameter of SnSe are lower than those of Pb Q ($Q = \text{Te, Se, S}$). The large Grüneisen parameter in PbTe is ascribed to the recent discovery that the Pb atoms are in fact somewhat displaced off the octahedron center in the rocksalt structure and the displacement increases with rising temperature [49]. The large Grüneisen parameter $\gamma \sim 3.13$ of SnSe confirms its large bond anharmonicity. Figure 5 gives a brief view of the crystal structure of SnSe and Pb Q ($Q = \text{Te, Se, S}$). Compared with the rigid bonds in the Pb Q ($Q = \text{Te, Se, S}$) system, SnSe possesses a weak chemical bond and

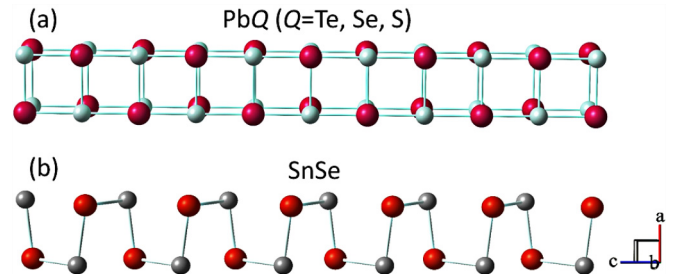


FIG. 5. The crystal structures of (a) Pb Q ($Q = \text{Te, Se, S}$) [1] and (b) SnSe [12]. Gray: Sn or Pb atoms; red: Te, Se, or S atoms.

a springlike crystal structure. Generally, weak bond stiffness will result in a soft phonon model and strong phonon vibrations during the heat transmission. The crystal structure of SnSe is featured by significantly distorted SnSe_7 polyhedra and a zigzag accordionlike geometry of slabs in the b - c plane. Along the a direction, the soft interatomic forces may result from the weak London forces that connect the strong-covalent-bond layers in SnSe. Moreover, the outermost two $5p$ electrons in Sn transfer to the $4p$ orbital of Se during forming Sn-Se bonds, which leaves the two $5s$ electrons in Sn as lone-pair electrons. The electrostatic repulsion between Sn lone-pair electrons and the bonding charges in Sn-Se bonds could weaken the resorting force during atomic vibrations (the soft acoustic modes in SnSe, Fig. 2), resulting in large bond anharmonicity. Recently, Li *et al.* reported that the large anharmonicity of SnSe is due to the long-range resonant network of Se p bonds coupled to active Sn $5s$ orbitals [16,17]. These bonds suffer from an instability that results in a particular temperature dependence of the force constants. The present results indicate that the low Young's modulus, low shear modulus, and large Grüneisen parameter reflect “soft” bonding in SnSe; these are the origins of ultralow lattice thermal conductivity.

In summary, we provide direct evidence to understand the origins of low thermal conductivity in SnSe using elastic

measurements. The obtained low average sound velocity, Young's modulus, and shear modulus illustrate the weak bond strength of SnSe, while the large Grüneisen parameter implies the strong anharmonicity of the chemical bonding arrangements and springlike crystal structure. The experimental measurements are well supported by the theoretical elastic and phonon calculations. Our work not only provides a solid complement to understand the low lattice thermal conductivity of SnSe, but also indicates thermoelectric materials with low thermal conductivity could have a decent research potential.

This work was supported by the “Zhuoyue” Program from Beihang University, the Recruitment Program for Young Professionals, National Natural Science Foundation of China under Grants No. 51571007 and No. 11474283; the Fundamental Research Funds for the Central Universities; the Major/Innovative Program of Development Foundation of Hefei Center for Physical Science and Technology, Grant No. 2014FXCX001; and the Science, Technology and Innovation Commission of Shenzhen Municipality (Grants No. ZDSYS20141118160434515 and No. JCYJ20140612140151884).

-
- [1] L. D. Zhao, V. P. Dravid, and M. G. Kanatzidis, *Energy Environ. Sci.* **7**, 251 (2014).
 - [2] X. Zhang and L.-D. Zhao, *J. Materomics* **1**, 92 (2015).
 - [3] Y. Z. Pei, X. Y. Shi, A. LaLonde, H. Wang, L. D. Chen, and G. J. Snyder, *Nature* **473**, 66 (2011).
 - [4] J. P. Heremans, V. Jovovic, E. S. Toberer, A. Saramat, K. Kurosaki, A. Charoenphakdee, S. Yamanaka, and G. J. Snyder, *Science* **321**, 554 (2008).
 - [5] T. J. Zhu, C. G. Fu, H. H. Xie, Y. T. Liu, and X. B. Zhao, *Adv. Energy Mater.* **5**, 1500588 (2015).
 - [6] K. F. Hsu, S. Loo, F. Guo, W. Chen, J. S. Dyck, C. Uher, T. Hogan, E. K. Polychroniadis, and M. G. Kanatzidis, *Science* **303**, 818 (2004).
 - [7] K. Biswas, J. Q. He, I. D. Blum, C. I. Wu, T. P. Hogan, D. N. Seidman, V. P. Dravid, and M. G. Kanatzidis, *Nature* **489**, 414 (2012).
 - [8] X. Shi and L. D. Chen, *Nat. Mater.* **15**, 691 (2016).
 - [9] W. G. Zeier, A. Zevalkink, Z. M. Gibbs, G. Hautier, M. G. Kanatzidis, and G. J. Snyder, *Angew. Chem., Int. Ed.* **55**, 6826 (2016).
 - [10] J. P. Heremans, M. S. Dresselhaus, L. E. Bell, and D. T. Morelli, *Nat. Nanotechnol.* **8**, 471 (2013).
 - [11] L. D. Zhao, J. Q. He, D. Berardan, Y. H. Lin, J. F. Li, C. W. Nan, and N. Dragoe, *Energy Environ. Sci.* **7**, 2900 (2014).
 - [12] L. D. Zhao, S. H. Lo, Y. Zhang, H. Sun, G. Tan, C. Uher, C. Wolverton, V. P. Dravid, and M. G. Kanatzidis, *Nature* **508**, 373 (2014).
 - [13] D. T. Morelli, V. Jovovic, and J. P. Heremans, *Phys. Rev. Lett.* **101**, 035901 (2008).
 - [14] X. Lu, D. T. Morelli, Y. Xia, F. Zhou, V. Ozolins, H. Chi, X. Zhou, and C. Uher, *Adv. Energy Mater.* **3**, 342 (2013).
 - [15] J. P. Heremans, *Nature* **508**, 327 (2014).
 - [16] J. P. Heremans, *Nat. Phys.* **11**, 990 (2015).
 - [17] C. W. Li, J. Hong, A. F. May, D. Bansal, S. Chi, T. Hong, G. Ehlers, and O. Delaire, *Nat. Phys.* **11**, 1063 (2015).
 - [18] D. W. Yang, X. L. Su, Y. G. Yan, T. Z. Hu, H. Y. Xie, J. He, C. Uher, M. G. Kanatzidis, and X. F. Tang, *Chem. Mater.* **28**, 4628 (2016).
 - [19] D. Y. Chung, T. Hogan, P. Brazis, M. Rocci-Lane, C. Kannewurf, M. Bastea, C. Uher, and M. G. Kanatzidis, *Science* **287**, 1024 (2000).
 - [20] H. L. Liu, X. Shi, F. F. Xu, L. L. Zhang, W. Q. Zhang, L. D. Cheng, Q. Li, C. Uher, T. Day, and G. J. Snyder, *Nat. Mater.* **11**, 422 (2012).
 - [21] D. D. Li, H. Z. Zhao, S. M. Li, B. P. Wei, J. Shuai, C. L. Shi, X. K. Xi, P. J. Sun, S. Meng, L. Gu, Z. F. Ren, and X. L. Chen, *Adv. Funct. Mater.* **25**, 6478 (2015).
 - [22] S. R. Brown, S. M. Kauzlarich, F. Gascoin, and G. J. Snyder, *Chem. Mater.* **18**, 1873 (2006).
 - [23] K. Kurosaki, A. Kosuga, H. Muta, M. Uno, and S. Yamanaka, *Appl. Phys. Lett.* **87**, 061919 (2005).
 - [24] M. D. Nielsen, V. Ozolins, and J. P. Heremans, *Energy Environ. Sci.* **6**, 570 (2013).
 - [25] L. D. Zhao, G. J. Tan, S. Q. Hao, J. Q. He, Y. L. Pei, H. Chi, H. Wang, S. K. Gong, H. B. Xu, V. P. Dravid, C. Uher, G. J. Snyder, C. Wolverton, and M. G. Kanatzidis, *Science* **351**, 141 (2016).
 - [26] K. Behnia, *Science* **351**, 124 (2016).
 - [27] K. L. Peng, X. Lu, H. Zhan, S. Hui, X. D. Tang, G. W. Wang, J. Y. Dai, C. Uher, G. Y. Wang, and X. Y. Zhou, *Energy Environ. Sci.* **9**, 454 (2016).
 - [28] C. L. Chen, H. Wang, Y. Y. Chen, T. Day, and G. J. Snyder, *J. Mater. Chem. A* **2**, 11171 (2014).
 - [29] T.-R. Wei, G. Tan, X. Zhang, C.-F. Wu, J.-F. Li, V. P. Dravid, G. J. Snyder, and M. G. Kanatzidis, *J. Am. Chem. Soc.* **138**, 8875 (2016).

- [30] O. Delaire, J. Ma, K. Marty, A. F. McGuire, M. H. Du, D. J. Singh, A. Podlesnyak, G. Ehlers, M. D. Lumsden, and B. C. Sles, *Nat. Mater.* **10**, 614 (2011).
- [31] Y. Zhang, X. Ke, P. R. C. Kent, J. Yang, and C. Chen, *Phys. Rev. Lett.* **107**, 175503 (2011).
- [32] See Supplemental Material at <http://link.aps.org/supplemental/10.1103/PhysRevB.94.125203> for experimental details and theoretical calculations of SnSe and Pb Q (Q = Te, Se, S).
- [33] Q. Zhang, E. K. Chere, J. Sun, F. Cao, K. Dahal, S. Chen, G. Chen, and Z. Ren, *Adv. Energy Mater.* **5**, 1500360 (2015).
- [34] G. Kresse and D. Joubert, *Phys. Rev. B* **59**, 1758 (1999).
- [35] J. P. Perdew, K. Burke, and M. Ernzerhof, *Phys. Rev. Lett.* **77**, 3865 (1996).
- [36] H. J. Monkhorst and J. D. Pack, *Phys. Rev. B* **13**, 5188 (1976).
- [37] J. M. J. den Toonder, J. A. W. van Dommelen, and F. P. T. Baaijens, *Modell. Simul. Mater. Sci. Eng.* **7**, 909 (1999).
- [38] A. Togo, F. Oba, and I. Tanaka, *Phys. Rev. B* **78**, 134106 (2008).
- [39] D. R. Clarke, *Surf. Coat. Technol.* **163**, 67 (2003).
- [40] H. Wang, E. Schechtel, Y. Z. Pei, and G. J. Snyder, *Adv. Energy Mater.* **3**, 488 (2013).
- [41] H. Wang, Y. Z. Pei, A. D. LaLonde, and G. J. Snyder, *Adv. Mater.* **23**, 1366 (2011).
- [42] R. Berman, *Thermal Conduction in Solids*, Oxford Studies in Physics (Clarendon Press, Oxford, UK, 1976).
- [43] C. L. Wan, W. Pan, Q. Xu, Y. X. Qin, J. D. Wang, Z. X. Qu, and M. H. Fang, *Phys. Rev. B* **74**, 144109 (2006).
- [44] Y.-L. Pei, J. Q. He, J. F. Li, F. Li, Q. J. Liu, W. Pan, C. Barreteau, D. Berardan, N. Dragoe, and L. D. Zhao, *NPG Asia Mater.* **5**, e47 (2013).
- [45] C. L. Wan, Z. X. Qu, Y. He, D. Luan, and W. Pan, *Phys. Rev. Lett.* **101**, 085901 (2008).
- [46] D. S. Sanditov and V. N. Belomestnykh, *Tech. Phys.* **56**, 1619 (2011).
- [47] J. Y. Cho, X. Shi, J. R. Salvador, G. P. Meisner, J. Yang, H. Wang, A. A. Wereszczak, X. Zhou, and C. Uher, *Phys. Rev. B* **84**, 085207 (2011).
- [48] E. J. Skoug and D. T. Morelli, *Phys. Rev. Lett.* **107**, 235901 (2011).
- [49] E. S. Bozin, C. D. Malliakas, P. Souvatzis, T. Proffen, N. A. Spaldin, M. G. Kanatzidis, and S. J. L. Billinge, *Science* **330**, 1660 (2010).